# Femtosecond-laser-written optofluidics in alumino-borosilicate glass

Andrea Crespi[a,b], Roberto Osellame[b,a], Francesca Bragheri[b,*]

[a] *Dipartimento di Fisica - Politecnico di Milano, p.za Leonardo da Vinci 32, 20133 Milano, Italy*
[b] *Istituto di Fotonica e Nanotecnologie - Consiglio Nazionale delle Ricerche, p.za Leonardo da Vinci 32, 20133 Milano, Italy*

**Abstract**

Femtosecond Laser Irradiation followed by Chemical Etching (FLICE) is a powerful technique for prototyping three-dimensional microfluidic structures in glass. Direct inscription of optical waveguides, by the same femtosecond laser, enables rapid fabrication of optofluidic devices for chemistry or biology applications. As a matter of fact, substrates where FLICE is known as most effective, such as fused silica, are not optimal for laser inscription of high-contrast optical waveguides, thus limiting the potentials of this technology. Here we show that it is possible to apply FLICE also to a commercial alumino-borosilicate glass, where very complex and low-loss photonic circuitry has been demonstrated recently. Besides optimizing the irradiation parameters to achieve hollow structures with high aspect-ratio, we investigate the etching dynamics and the micro-morphology of the etched regions. As a test for the technique, we realize an optofluidic device composed of a microchannel and two intersecting optical waveguides.

*Keywords:* femtosecond laser micromachining, microfluidics, borosilicate glass

*Corresponding author
*Email address:* francesca.bragheri@ifn.cnr.it (Francesca Bragheri)

## 1. Introduction

Ultrafast lasers are exceptionally versatile tools for micromachining transparent dielectric materials.[1] Femtosecond laser pulses can be exploited for ablation, drilling, dicing, or welding, but they present also more peculiar machining capabilities such as optical waveguide writing,[2] or microchannel realization when a chemical etching step is added as in the FLICE technique[3, 4]. According to the latter method, tracks with arbitrary paths are laser-inscribed in the bulk substrate and subsequently exposed to a proper chemical agent (typically hydrofluoric acid or potassium hydroxide). Such tracks yield a higher etching rate with respect to the raw substrate, thus enabling buried microchannels or other hollow structures of arbitrary three-dimensional shapes to be excavated in the substrate with high precision.

As a matter of fact, FLICE technique has been applied to a limited set of substrates, which include fused silica[5, 6], Foturan (Schott) glass[7] and a few crystals[8] among the most prominent examples[9]. In particular, in fused silica the etching rate of laser-irradiated glass can be hundreds of times larger than the one of the pristine substrate[5, 10], making it possible to realize millimetre-sized buried microchannels and other etched structures with high aspect ratios (A.R.). In addition, in such substrate FLICE can be combined straightforwardly with femtosecond laser waveguide writing, enabling a range of applications in optofluidics[11], including biological sensing[12, 13] and cellomics[14, 15, 16]. Indeed, it is possible to realize optofluidic devices where microchannels are monolithically integrated with optical waveguides, using a single laser irradiation step and thus taking advantage of an intrinsic and precise relative alignment.

Actually, achieving optical waveguides that yield reasonably low propagation loss ($< 1$ dB/cm) and index contrasts comparable to the one of optical fibers is not trivial in fused silica, and typically require long machining times[17, 18]. This poses limitations to the complexity of the optical circuits that can be interfaced with the fluidic channels. On the other hand, waveguides with index contrast approaching $1 \cdot 10^{-2}$ and propagation loss $< 0.3$ dB/cm have been

demonstrated in Eagle alumino-borosilicate glass (Corning), where the scanning speeds required in the laser-irradiation process are usually one or two order of magnitudes faster than in fused silica [19]. In the same substrate, complex circuits have been reported recently, presenting the high optical quality needed to support single-photon operation, and including reconfiguration capabilities.[20, 21]

In this work we demonstrate the successful application of the FLICE technique also to Eagle XG substrates. In detail, we investigate a wide range of laser irradiation parameters to optimize the etching selectivity, and we observe how the increased etching rates are related to morphologic features of the laser modified track. We finally demonstrate a simple optofluidic device, entirely realized by femtosecond laser pulses.

## 2. Methods

The laser source employed is a Yb:KYW cavity-dumped mode-locked laser oscillator, delivering ∼300 fs pulses at 1 MHz repetition rate, with a wavelength of 1030 nm. In our experiments the beam is focused in the glass by a 50× microscope objective (NA = 0.6) and inscription power is finely adjusted by rotating a half-waveplate, followed by a linear polarizer.

To inscribe the tracks, the Eagle XG glass sample is fixed onto a three-axis air-bearing translation system (Aerotech FiberGLIDE), which allows translation velocities up to 300 mm/s with a precision in positioning lower than 100 nm. The relative orientation of the laser polarization with respect to the translation direction is chosen either by properly rotating the linear polarizer in the beam line, or by varying the translation direction.

The wet etching process is performed by immersing each glass sample in a beaker containing 50 ml of aqueous solution of hydrofluoric acid (5% concentration). The beaker is placed in an ultrasonic bath and the temperature is kept constant at 35° C. While other chemical agents, such as e.g. potassium hydroxide, would possibly provide higher etching selectivity[10], we choose to

employ hydrofluoric acid in this study because etching rates of glass are order of magnitudes larger. This makes it convenient for a time-efficient investigation of the process.

## 3. Results

### *3.1. Optimization of irradiation parameters*

As a first experiment, we explored the etching dynamics for a wide range of irradiation parameters, in terms of power and translation speeds. In detail, several sets of tracks were written, with powers and scan speeds ranging respectively from 100 mW to 600 mW and from 1 mm/s to 100 mm/s; the laser beam was focused 170 $\mu$m below the top surface of the glass and polarization was kept orthogonal to the translation direction. The same sets of tracks were then inscribed also with the laser polarization parallel to the translation direction. Upon inspection with an optical microscope, right after the laser fabrication process, no relevant modifications of the glass were observed for $P = 100$ mW. Visible traces are discernible, instead, for higher writing powers. After 40 minutes of etching, excavated cones of various lengths and base radii are observed along the laser-written tracks. In our experimental conditions the A.R. of the cones, i.e. length over radius, gives an estimate of the ratio between the etching rate of the irradiated track over the etching rate of the bulk glass (see Appendix A). Figure 1 summarizes the achieved results: the graph shows that cones with high A.R. are concentrated preferentially in the region of powers larger than 300 mW and speeds larger than 30 mm/s.

Three regions can be clearly identified: for slow speeds and low powers (region I) we observe just a slight increase of the etching rate along the laser written tracks, with A.R. $< 2$ for both irradiation polarizations. For larger speeds and powers, we observe an intermediate regime (region II) in which only the tracks irradiated with orthogonal polarization experience a significant increase of the etching rate with respect to the bulk. Finally, in region III, i.e. for the highest translation speeds, we observe A.R. $> 6$ independently from

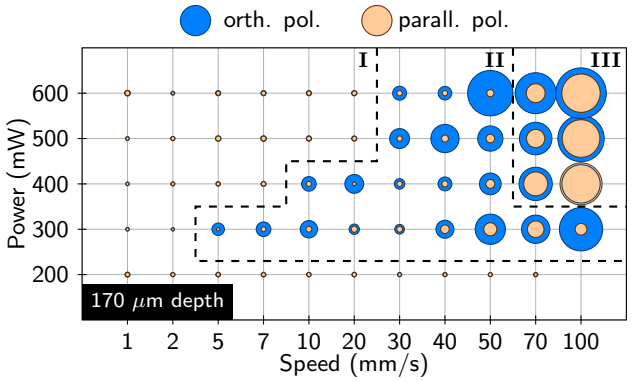


Figure 1: A.R. of cones etched along laser-inscribed tracks written at 170 $\mu$m depth, as a function of the irradiation parameters (power, translation speed, polarization of the laser beam). The radius of the circles is proportional to the ratio between the length of the cone and its radius, as measured after 40 minutes of etching. The size of the circles in the legend corresponds to a value of 10.

the irradiation polarization, with a maximum A.R. $\simeq$ 17 for the tracks written with 600 mW power, 100 mm/s translation speed and orthogonal polarization. We also observe that the etched cones produced in regime III typically look smoother and more uniform than the ones obtained in the regime II, which are mostly of irregular profile. Microscope pictures of the etched cones in different regimes are shown in Figs. 2(a-f).

As a second experiment, we investigated in more detail the capabilities of the etching process, with the aim of fabricating microfluidic devices. We are therefore mainly interested in optimizing the fabrication conditions that produce smooth and elongated cones, deep in the glass substrate. This indeed would allow one to etch large apertures to insert micro-tubing for the connection to the external fluidic network.

On the basis of the first results, we irradiated a set of tracks with high velocities (from 30 mm/s to 100 mm/s) and high powers (from 400 mW to 800 mW), at 500 $\mu$m depth in the substrate and keeping the laser polarization perpendicular to the translation direction. We increased the power up to 800 mW to possibly allow for a compensation of the increased aberrations in the focus,

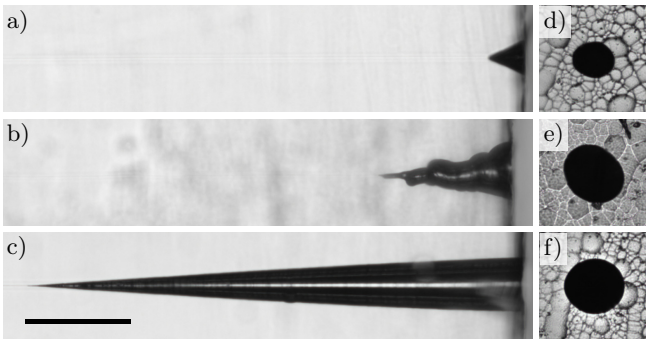


Figure 2: Examples of etched cones (top and side views) fabricated at 170 $\mu$m depth with irradiation parameters of: $P = 400$ mW, $v = 40$ mm/s, parallel polarization (panels (a) and (d)); $P = 400$ mW, $v = 40$ mm/s, orthogonal polarization (panels (b) and (e)); $P = 600$ mW, $v = 70$ mm/s, orthogonal polarization (panels (c) and (f)). Scalebar is 150 $\mu$m.

caused by the larger inscription depth. To accurately characterize the etching process we performed it in three steps of 40 minutes each.

The obtained results confirm that the highest A.R., i.e. the highest etching rates of the irradiated track, are reached for the largest speeds and powers (see Figs. 3 and 4). In particular, for speeds $v$ = 50-100 mm/s and powers $P$ =600-800 mW the etching rates of the track in the first 40 minutes of etching is about 800-900 $\mu$m/h, i.e. 13-15 times the etching rate of the bulk material which is about 60 $\mu$m/h. For these parameters, the etched cones are smooth and have a very regular profile, similar to that of Fig. 2(c). The cone inlet is approximately circular, with an ellipticity (ratio between vertical and horizontal diameter) smaller than 1.2.

The measured etching rates tend indeed to decrease with time, leading to a maximum observed cone length of about 800 $\mu$m, quite independently from the irradiation parameters. The cone diameter at its entrance, on the other hand, keeps enlarging, leading to a decrease in the A.R.. This may be explained by the limited diffusion of acid molecules in solution, inside a deep and narrow cone. In fact, while the acid diffuses towards the tip of the cone it is consumed by the reaction with the glass at the walls. This causes a decreasing gradient of the concentration from the entrance, where it can be assumed to be constant,

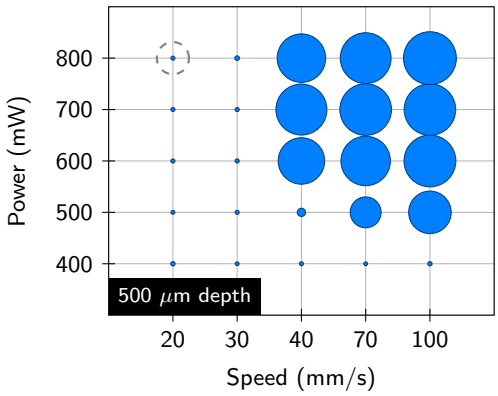


Figure 3: A.R. of cones etched along laser-inscribed tracks written at 500 $\mu$m depth, with polarization orthogonal to the translation direction, as a function of the other irradiation parameters (power, translation speed). The radius of the blue circles is proportional to the ratio between the length of the cone and its radius, as measured after 40 minutes of etching. The dashed gray circle indicates the size corresponding to a value of 10.

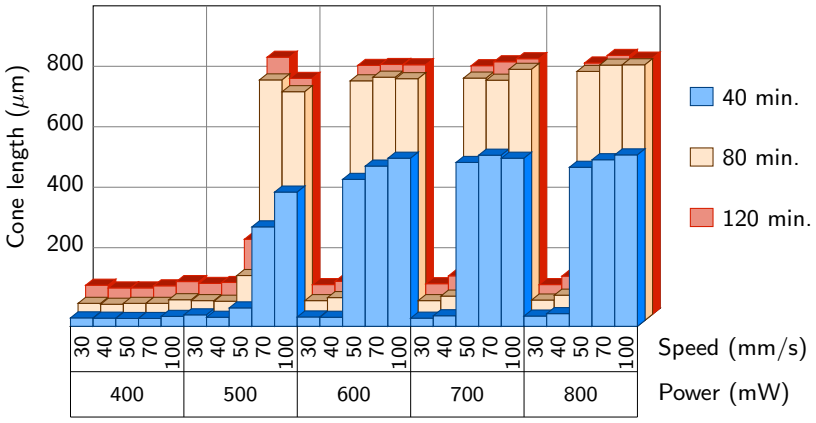


Figure 4: Length of the etched cones as a function of the irradiation parameters and of the etching time. Tracks were irradiated at 500 $\mu$m depth in the substrate, with the laser polarization orthogonal to the translation direction.

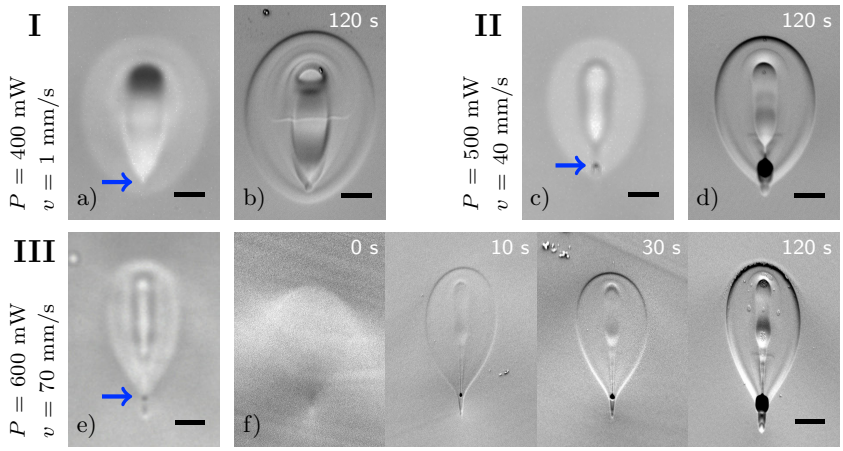


Figure 5: Cross-section of tracks inscribed with different parameters as indicated, with polarization of the writing beam orthogonal to the translation. They belong to the three different etching regimes. Tracks I and II are inscribed at a depth of 170 $\mu$m below the glass surface, track III at a depth of 500 $\mu$m. Panels (a), (c) and (e) are pictures taken with an optical microscope, panels (b), (d), (f) report images acquired with a SEM, at different etching times, as reported in the labels. The SEM pictures were acquired using a sample-holder tilted by 45° to enhance contrast; images have been stretched by a factor of $\sqrt{2}$ along the vertical direction to facilitate comparison with the microscope picture. All scale bars correspond to 5 $\mu$m. Blue arrows indicate the position of the laser focus in the irradiation process.

to the tip of the cone (see also a simple physical discussion in Appendix B). As a result, the advancement rate of the tip of the channel will slow down up to the point at which the rate at the tip equals the rate of the external surface of the glass, thus leading to a saturation of the total length of the channel. On the other hand, the cone base will tend to enlarge at a fixed rate, because the acid concentration at the inlet does not change.

### *3.2. Investigation of the etching mechanism*

The etching process appears related to specific features in the morphology of the written tracks, as they appear at the optical microscope before etching. Examples of cross-sections of tracks written with different parameters and belonging to the three regimes discussed in Section 3.1 are reported in Fig. 5(a),(c),(e). The cross-sections present in general a complex structure, in agreement with

previous studies of femtosecond laser written waveguides in borosilicate glass at 1 MHz repetition rate. [22, 23] In detail, an elliptical central region of melted and resolidified material is surrounded by a thermally modified crown. A very small but definite black dot is observed at the bottom of the cross-section, as noted already by Eaton et al. [23], in correspondence of the focal position. Notably, from our results the presence of this black dot is a necessary condition to experience a significant etching-rate increase with respect to the bulk glass. In fact, it is present in all tracks belonging to regime II or III, while it is typically absent in tracks belonging to regime I.

The cross-section of the etched cones, in regimes I and II, indeed follows quite closely the elliptical shape of the modified track. In regime III is instead more circular, as mentioned already. This might begin to suggest that the cone excavation, in the latter case, proceeds from a small point inside the cross-section rather than from an enhanced etching sensitivization of the whole modified region.

To get some deeper insight on the etching mechanism, we inscribed several tracks with the three different parameters indicated in Fig. 5. We cleaved the sample, transversally to the tracks, in several pieces and each piece was immersed in the acid solution for a different duration, ranging from 0 s to about 120 s. The cleaved and etched facets were then sputter-coated with a $\sim$10 nm gold layer and analyzed with a scanning electron microscope (SEM); see Fig. 5(b),(d),(f). Let us discuss in some more detail the process observed in the case of regime-III tracks, for which we report the SEM images for different etching times in Fig. 5(f). A distinct hole with the size of approximately 500 nm appears at the bottom of the cross-section, even for the shortest etching time. This hole is placed in perfect correspondence with the black dot noticed at the optical microscope. With increased etching times the hole enlarges progressively and is the main responsible for the excavation of the microchannel. The other regions of the cross-section also yield a modulated etching rate, which testifies the different alterations of the glass structure. However, the hole at the bottom gets immediately much deeper than the rest of the section.

We note that this morphology is utterly different from the typical one observed in the case of fused silica, where most part of the irradiated cross-section yields a highly increased etching rate, in the order of tens of times the one measured for bulk glass, and periodic polarization-dependent nano-structures are displayed [6]. Nanogratings have been indeed observed also in laser processing of other type of glasses [24, 25]. Here, the chemical etching proceeds mostly from a point-like feature up to the resolution of our instruments. Nanogratings are not apparent and we do not observe the strong polarization dependency of the etching rate typically associated to the nanograting-driven etching regime [26].

Further study is required to ascertain the microscopic structure of this peculiar laser-induced modification. Actually, direct investigation with optical or electronic spectroscopic techniques may not be easy, because of the extremely small size of this feature, which is well below 1 $\mu$m.

As a matter of fact, we might conjecture that the black dot visible in the cross-section is a micro-crack or rupture in the material, practically continuous along all the irradiated track, caused by the mechanical stresses that occur in the femtosecond laser irradiation process. The presence of stresses around the irradiated cross-section, particularly concentrated in the bottom part, is supported by the ondulation of the cleaved glass surface visible in Fig. 5(f) for null etching time, where no definite hole is yet visible. In fact, after irradiation and before immersion in the etching bath, the crack is of negligible width, but it may be rapidly enlarged due to the preferential penetration of the acid. This interpretation may be compatible with the experimental fact that the enhanced etching rates are measured for the highest laser pulse energies and scanning speeds. On the one side, a too small pulse energy may not be sufficient to induce such a disruptive phenomenon. On the other side, high speeds may be required to avoid remelting the material. A large molten core, as is formed due to thermal accumulation at low speeds, might also behave as an elastic body that helps in quenching stresses and avoid cracking [27].

Finally, we may devote a comment to the presence of a sort of transition re-

gion towards such favourable modification regime, in the space of the irradiation parameters, which is region II in Fig. 1. As already mentioned, in this region we observe at the microscope the black-dot in the cross-section (Fig. 5c) but the etched cones may appear with irregular shapes (Fig. 2b). In addition, we observe a moderate dependence on the direction of the laser polarization, which practically disappears in region III. We may interpret this transition region as a condition in which the micro-crack begins to be formed but is irregular and discontinuous, or not homogeneous enough. At such a threshold condition even small changes in the microscopic interaction dynamics, such as those given by changing the polarization direction, may appear more evidently. In fact, formation of polarization dependent microstructures have been reported also in alumino-silicate glasses even in the presence of strong thermal phenomena [28], which have been attributed to anisotropic reflections of the laser light within the modified region during the modification process itself.

### *3.3. An optofluidic prototype device*

Finally, to provide a first demonstration of the microstructuring possibilities in Eagle XG glass for optofluidic applications, we designed and fabricated a device consisting in a hourglass-shaped microchannel interfaced with two orthogonal optical waveguides in the narrowest part. The hourglass channel has an overall length of 1.5 mm and reaches a diameter larger than 400 $\mu$m at the two entrances, to enable connectorization with capillary tubes (see Fig. 6(a)). The laser irradiated tracks and the waveguides were inscribed in a larger glass sample: the device footprint of 1.5 mm was defined with a diamond-wire saw and then the sample was put in the etching bath.

In fused silica glass, FLICE technology can take advantage of spiralling irradiation paths, in order to define with high resolution the shapes of the etched channels.[4] However, the scanning speeds required to irradiate etchable tracks in Eagle XG are tens of times higher than the typical scanning speeds in fused silica. Limitations in the translation stages acceleration would not allow us to irradiate small-radius helixes that define the hourglass shape with high detail.

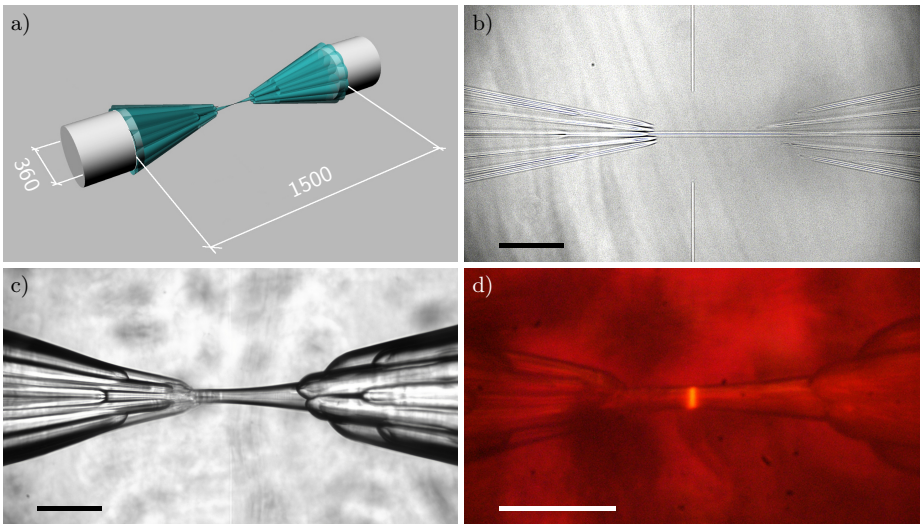


Figure 6: (a) Scheme of the hourglass-shaped microfluidic channel, built of the assembly of several etched cones. The white cylinders represent terminations of microfluidic tubes, inserted at the extremities of the channel. Dimensional quotes are in microns. Microscope pictures of optofluidic device, taken at different stages of the fabrication and testing processes. (b) Detail of the irradiated traces, towards the center of the channel. The optical waveguide is also visible, as a vertical line with an interruption around the central track of the channel. (c) Image of the final device (filled with acetone), as resulting after 70 minutes of etching. (d) Picture of the channel filled with rhodamine solution and green laser light coupled in one of the waveguide: orange fluorescence is clearly visible in the center of the channel. The picture is taken with a notch filter at the excitation wavelength. Scale bars are 200 $\mu$m.

Therefore, to produce the desired shape we chose to inscribe a set of straight segments, converging towards the center of the hourglass, plus one continuous straight track placed at the center of the channel as visible in Fig. 6(b). Irradiation parameters were $P = 600$ mW, $v = 70$ mm/s and polarization orthogonal to the translation direction. The combination of the etched cones, after 70 minutes of etching, produced the resulting shape shown in Fig. 6(c).

The optical waveguides were inscribed together with the etching tracks: irradiation parameters for the waveguides are $P = 280$ mW and $v = 10$ mm/s. These parameters give a single-mode behavior at about 1 $\mu$m wavelength and slight multimodality in the visible.

To test the device PEEK tubings (with 360 $\mu$m outer diameter) were inserted in the two inlets and fixed with a UV-curing glue, and rhodamine solution was flown in the channel. Green light (532 nm wavelength) from a DPSS frequency-doubled Nd:YAG laser was coupled into one of the waveguides. Figure 6(d) shows a microscope picture of the device, acquired using a notch filter at the green laser wavelength. The fluorescence emitted by the rhodamine is clearly visible only in the narrow region illuminated by the optical waveguide facing the microchannel.

## 4. Conclusions

We have demonstrated selective chemical etching of femtosecond laser written tracks in Eagle XG substrates. For the optimum parameters, the etching rate show low dependency on the polarization of the inscription laser beam. In addition, the highest etching rate results to be correlated to a point-like feature in the track cross section, rather than to a wider irradiated region. These elements suggest that the etching sensitivization rely on a different microscopic mechanism with respect to fused silica, even if further studies are required on this point.

A simple optofluidic structure has been also demonstrated, composed of a microchannel and an intersecting optical waveguide. Such structure is at the basis of several different optofluidic lab-on-a-chip devices, for diverse applications ranging from bio-chemical analysis[12], cellomics[14, 15, 16] and integrated microfluidic interferometry[13]. We thus believe that this work paves the way to more complex fluidic lab-on-a-chips, entirely fabricated by femtosecond laser micromachining, where a network of microchannels can be interfaced with elaborated and low-loss optical waveguide circuits.

We finally note that the scanning speeds in the irradiation steps, as well as the required etching times, are much faster than the typical ones for FLICE in fused silica. This provides further advantages in terms of rapid prototyping of optofluidic devices.

Work is ongoing in investigating the etching response of irradiated tracks with lower pulse-repetition rates, with the purpose of achieving good etching conditions also for lower irradiation speeds, which may be more convenient to produce microstructures with complex shapes. Future studies shall also involve different etching agents such as KOH, which yields lower etching rates with respect to HF, at comparable etchant concentrations. In fact, this may provide a more favourable reaction/diffusion balance, decrease saturation effects in the etching process and thus allows for the excavation of longer and higher-aspect-ratio microchannels.

**Acknowledgments**

This work was partially supported by the European Union's Horizon 2020 FET Open programme under the PROCHIP project (grant agreement no. 801336) and by the European Research Council (ERC) Advanced Grant CAPABLE (grant agreement no. 742745).

## References


[1] R. Gattass, E. Mazur, Femtosecond laser micromachining in transparent materials, Nat. Photonics 2 (4) (2008) 219–225.

[2] K. M. Davis, K. Miura, N. Sugimoto, K. Hirao, Writing waveguides in glass with a femtosecond laser, Opt. Lett. 21 (21) (1996) 1729–1731.

[3] A. Marcinkevičius, S. Juodkazis, M. Watanabe, M. Miwa, S. Matsuo, H. Misawa, J. Nishii, Femtosecond laser-assisted three-dimensional microfabrication in silica, Opt. Lett. 26 (5) (2001) 277–279.

[4] K. Vishnubhatla, N. Bellini, R. Ramponi, G. Cerullo, R. Osellame, Shape control of microchannels fabricated in fused silica by femtosecond laser irradiation and chemical etching, Opt. Express 17 (10) (2009) 8685–8695.

[5] Y. Bellouard, A. Said, M. Dugan, P. Bado, Fabrication of high-aspect ratio, micro-fluidic channels and tunnels using femtosecond laser pulses and chemical etching, Opt. Express 12 (10) (2004) 2120–2129.

[6] C. Hnatovsky, R. Taylor, E. Simova, P. Rajeev, D. Rayner, V. Bhardwaj, P. Corkum, Fabrication of microchannels in glass using focused femtosecond laser radiation and selective chemical etching, Appl. Phys. A 84 (2006) 47–61.

[7] Y. Cheng, K. Sugioka, K. Midorikawa, M. Masuda, K. Toyoda, M. Kawachi, K. Shihoyama, Control of the cross-sectional shape of a hollow microchannel embedded in photostructurable glass by use of a femtosecond laser, Opt. Lett. 28 (1) (2003) 55–57.

[8] A. Ródenas, M. Gu, G. Corrielli, P. Paiè, S. John, A. K. Kar, R. Osellame, Three-dimensional femtosecond laser nanolithography of crystals, Nat. Photonics 13 (2) (2019) 105.

[9] J. Gottmann, M. Hermans, N. Repiev, J. Ortmann, Selective laser-induced etching of 3d precision quartz glass components for microfluidic

applicationsup-scaling of complexity and speed, Micromachines 8 (4) (2017) 110.

[10] S. Kiyama, S. Matsuo, S. Hashimoto, Y. Morihira, Examination of etching agent and etching mechanism on femotosecond laser microfabrication of channels inside vitreous silica substrates, J. Phys. Chem. C 113 (27) (2009) 11560–11566.

[11] R. Osellame, H. Hoekstra, G. Cerullo, M. Pollnau, Femtosecond laser microstructuring: an enabling tool for optofluidic lab-on-chips, Laser Photonics Rev. 5 (3) (2011) 442–463.

[12] R. Martinez-Vazquez, R. Osellame, M. Cretich, M. Chiari, C. Dongre, H. J. Hoekstra, M. Pollnau, H. van den Vlekkert, R. Ramponi, G. Cerullo, Optical sensing in microfluidic lab-on-a-chip by femtosecond-laser-written waveguides, Anal. Bioanal. Chem. 393 (4) (2009) 1209.

[13] A. Crespi, Y. Gu, B. Ngamsom, H. Hoekstra, C. Dongre, M. Pollnau, R. Ramponi, H. van den Vlekkert, P. Watts, G. Cerullo, R. Osellame, Three-dimensional mach-zehnder interferometer in a microfluidic chip for spatially-resolved label-free detection, Lab. Chip 10 (2010) 1167–1173.

[14] M. Kim, D. J. Hwang, H. Jeon, K. Hiromatsu, C. P. Grigoropoulos, Single cell detection using a glass-based optofluidic device fabricated by femtosecond laser pulses, Lab Chip 9 (2) (2009) 311–318.

[15] N. Bellini, K. Vishnubhatla, F. Bragheri, L. Ferrara, P. Minzioni, R. Ramponi, I. Cristiani, R. Osellame, Femtosecond laser fabricated monolithic chip for optical trapping and stretching of single cells, Opt. Express 18 (5) (2010) 4679–4688.

[16] P. Paiè, F. Bragheri, R. M. Vazquez, R. Osellame, Straightforward 3d hydrodynamic focusing in femtosecond laser fabricated microfluidic channels, Lab Chip 14 (11) (2014) 1826–1833.

[17] S. M. Eaton, M. L. Ng, R. Osellame, P. R. Herman, High refractive index contrast in fused silica waveguides by tightly focused, high-repetition rate femtosecond laser, J. Non-Cryst. Solids 357 (11-13) (2011) 2387–2391.

[18] J. Guan, X. Liu, P. S. Salter, M. J. Booth, Hybrid laser written waveguides in fused silica for low loss and polarization independence, Opt. Express 25 (5) (2017) 4845–4859.

[19] A. Arriola, S. Gross, N. Jovanovic, N. Charles, P. G. Tuthill, S. M. Olaizola, A. Fuerbach, M. J. Withford, Low bend loss waveguides enable compact, efficient 3d photonic chips, Opt. Express 21 (2013) 2978–2986.

[20] Z. Chaboyer, T. Meany, L. Helt, M. J. Withford, M. Steel, Tunable quantum interference in a 3d integrated circuit, Sci. Rep. 5 (2015) 9601.

[21] A. Crespi, M. Bentivegna, I. Pitsios, D. Rusca, D. Poderini, G. Carvacho, V. DAmbrosio, A. Cabello, F. Sciarrino, R. Osellame, Single-photon quantum contextuality on a chip, ACS Photonics 4 (11) (2017) 2807–2812.

[22] S. Eaton, H. Zhang, P. Herman, F. Yoshino, L. Shah, J. Bovatsek, A. Arai, Heat accumulation effects in femtosecond laser-written waveguides with variable repetition rate, Opt. Express 13 (12) (2005) 4708–4716.

[23] S. M. Eaton, H. Zhang, M. L. Ng, J. Li, W.-J. Chen, S. Ho, P. R. Herman, Transition from thermal diffusion to heat accumulation in high repetition rate femtosecond laser writing of buried optical waveguides, Opt. Express 16 (13) (2008) 9443–9458.

[24] N. Varkentina, T. Cardinal, F. Moroté, P. Mounaix, P. André, Y. Deshayes, L. Canioni, Examination of femtosecond laser matter interaction in multipulse regime for surface nanopatterning of vitreous substrates, Opt. Express 21 (24) (2013) 29090–29100.

[25] S. Richter, C. Miese, S. Döring, F. Zimmermann, M. J. Withford, A. Tünnermann, S. Nolte, Laser induced nanogratings beyond fused silica-

periodic nanostructures in borosilicate glasses and ule, Opt. Mater. Express 3 (8) (2013) 1161–1166.

[26] C. Hnatovsky, R. Taylor, E. Simova, V. Bhardwaj, D. Rayner, P. Corkum, Polarization-selective etching in femtosecond laser-assisted microfluidic channel fabrication in fused silica, Opt. Lett. 30 (14) (2005) 1867–1869.

[27] I. Miyamoto, K. Cvecek, M. Schmidt, Crack-free conditions in welding of glass by ultrashort laser pulse, Opt. Express 21 (12) (2013) 14291–14302.

[28] F. Zhang, M. Gecevičius, Q. Chen, H. Zhang, Y. Dai, J. Qiu, Evolution of polarization dependent microstructures induced by high repetition rate femtosecond laser irradiation in glass, Opt. Express 24 (19) (2016) 21353–21363.

## Appendix A. Aspect ratio of the etched cone

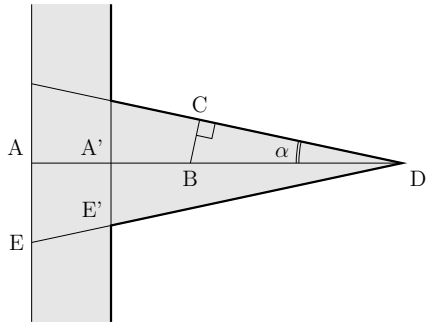


Figure A.7: Geometric scheme of the longitudinal section of an etched cone. Gray area indicates removed material.

To understand how the proportions of the etched cone are related to the etching rates of the bulk and of the irradiated glass, we can consider the enlargement of the cone during the etching process. In particular, we consider an etching process that proceeds at a rate $R$ in the bulk glass (we define the rate as the surface advancement per unit time) and at a rate $R^*$ along the central irradiated track.

The following simple model assumes the two etching rates as constant in time, and thus does not take into account the diffusion/reaction dynamics discussed in Appendix B. In addition, it is based on the approximation that the central irradiated track (or at least the part of the track that is more favourably etched) is much thinner than the actual diameter of the sections of the etched cone. The latter approximation may be not suitable if $R^*$ were several order of magnitudes larger than $R$: however, in the experimental conditions of the present work we have $R^* < 20R$, thus the model is appropriate.

Starting from the pristine sample surface, at the position A in Figure A.7, after a time $\tau$ the etchant has reached the point D, proceeding at the rate $R^*$ along the central line. We can write:

$$\overline{\mathrm{AD}} = R^* \tau \tag{A.1}$$

We can divide this path into two segments, $\overline{\mathrm{AB}}$ and $\overline{\mathrm{BD}}$, covered respectively in a time $\tau_1$ and $\tau_2$:

$$\overline{\mathrm{AB}} = R^*\tau_1 \qquad \overline{\mathrm{BD}} = R^*\tau_2 \qquad \text{with } \tau = \tau_1 + \tau_2 \tag{A.2}$$

We note that, in order to reach the point C, the etching should have proceeded up to B in the same time $\tau_1$ at a rate $R^*$, and then should have covered $\overline{\mathrm{BC}}$ in the time $\tau_2$ at a rate $R$:

$$\overline{\mathrm{BC}} = R\tau_2 \tag{A.3}$$

The walls of the cones should in fact advance, while enlarging the cone, proceeding parallel to themselves.

Considering now that $\overline{\mathrm{BC}} = \mathrm{BD} \cdot \sin\alpha$ we can write the equality:

$$R\tau_2 = R^*\tau_2 \sin\alpha \tag{A.4}$$

which means that the aperture angle of the cone is related to the ratio between the two etching rates:

$$\sin\alpha = \frac{R}{R^*} \tag{A.5}$$

The A.R. of the cone can be defined as the length of the cone over its radius, and corresponds to:

$$\text{A.R.} = \frac{\overline{\mathrm{A'D}}}{\mathrm{A'E'}} = \cot\alpha = \frac{1}{\tan\alpha} \tag{A.6}$$

Using $\sin^2\alpha = \frac{1}{\cot^2\alpha+1}$, we can write a compact relation between the ratio of the etching rates and the A.R. of the cone:

$$\frac{R^*}{R} = \frac{1}{\sin\alpha} = \sqrt{\cot^2\alpha + 1} = \sqrt{(\text{A.R.})^2 + 1} \tag{A.7}$$

## Appendix B. Diffusion of etchant in excavated microchannels

We derive in the following an approximate and very simple description of the balance between the diffusion and reaction mechanisms, within a thin microchannel with circular cross section, during the etching process. We reduce the problem to one dimension, assuming that the etchant concentration is a

function only of the longitudinal coordinate $c = c(x)$. This approximation is plausible in case of long and thin microchannels, while it may fall in case of larger ones.

To begin, let us consider diffusion phenomena alone. We divide the microchannel in small cylindrical segments of length $dx$ and radius $r$, and we focus on the segment placed at coordinate $x$. The cylindrical volume $\pi r^2\, dx$ contains a quantity of etchant $dN = c\,\pi r^2 dx$. Its variation in a time interval $dt$ will be given by the flux of etchant diffused from the adjacent segments. We can write:

$$\begin{aligned} dN_{left} &= \Phi_{left} dt = D\pi r^2 dt \frac{c(x-dx) - c(x)}{dx} \\ dN_{right} &= \Phi_{right} dt = D\pi r^2 dt \frac{c(x+dx) - c(x)}{dx} \end{aligned} \tag{B.1}$$

In fact, each of the two fluxes is assumed proportional, through a coefficient $D$, to the concentration gradient and to the cross-section area $\pi r^2$. The variation of etchant concentration per unit time is:

$$\frac{dc}{dt} = \frac{dN}{dt\ \pi r^2\, dx} = \frac{\Phi_{left} + \Phi_{right}}{\pi r^2\, dx} = D\,\frac{c(x-dx) - 2c(x) + c(x+dx)}{dx} \tag{B.2}$$

which is namely:

$$\frac{dc}{dt} = D\frac{d^2c}{dx^2} \tag{B.3}$$

The latter is indeed the classical diffusion equation in one dimension. Its stationary solution is a constant function:

$$c(x) = c_0 \tag{B.4}$$

This means that, if sufficient time is allowed in order to reach the stationary condition, the concentration inside the microchannel reaches the same concentration of the inlet (which has to be $c_0$) in each point.

As a matter of fact, along with the diffusion process in the microchannel, part of the etchant is consumed by the reaction at the walls. For the cylindrical volume of length $dx$ we may write, as a first approximation, an equivalent *flux* of etchant that is actually consumed by the reaction at the external surface of

area $2\pi r\,dx$. In a time $dt$ the quantity of substance consumed is:

$$dN_{react} = \Phi_{react}\,dt = -2\pi r\,dx \cdot c\frac{R}{2}dt \tag{B.5}$$

where, for the sake of simplicity, we have assumed a proportionality of the reaction dynamics to the first power of the concentration and to the first power of the available area, through a coefficient $\frac{R}{2}$. Now the balance equation reads:

$$\frac{dc}{dt} = \frac{dN}{dt\,\pi r^2\,dx} = \frac{\Phi_{left} + \Phi_{right} + \Phi_{react}}{\pi r^2\,dx} \tag{B.6}$$

$$\frac{dc}{dt} = D\frac{d^2c}{dx^2} - \frac{R}{r}c \tag{B.7}$$

i.e., the diffusion equation (B.3) is modified by adding a term proportional to $c$.

A very simple stationary solution of (B.7) is given in the case of a channel with constant radius $r_0$ and indefinite length. In detail, if we place the inlet (with the boundary condition $c = c_0$) at $x = 0$ we obtain:

$$c(x) = c_0 e^{-a\,x} \qquad \text{with} \qquad a = \sqrt{\frac{R}{r_0 D}}. \tag{B.8}$$

Therefore, in these conditions, the acid concentration decreases exponentially with the depth of the channel. Since the added term in (B.7), accounting for the reaction, is inversely proportionally to the radius $r$, the decrease in concentration will be even more steep in the case of a narrowing channel, e.g. a conical one.

Actually, the stationary equation has an exact analytic solution also in the case of a cone with length $L$ and initial radius $r_0$ (i.e. when $r = r_0(1x/L)$. In detail:

$$c(x) = K\sqrt{L-x} \cdot \mathrm{I}_1(2a\sqrt{L-x}) \tag{B.9}$$

where $\mathrm{I}_1$ is the modified Bessel function of the first kind (of order 1), $K$ is a proper constant to fit the initial condition $c(0) = c_0$ and $a = \sqrt{\frac{RL}{r_0 D}}$. Basically, $c(x)$ is a rapidly decreasing function, reaching zero at the tip of the channel. It should be noted, however, that in the latter description the tip is modeled as point-like and thus some unphysical condition may occur in that limit.